Title: High riverine CO_2 emissions at the permafrost boundary of Western Siberia

Authors: S. Serikova[1]*, O.S. Pokrovsky[2], P. Ala-Aho[3,4], V. Kazantsev[5], S.N. Kirpotin[6], S.G. Kopysov[7], I.V. Krickov[6], H. Laudon[8], R.M. Manasypov[6,9], L.S. Shirokova[2,9], C. Soulsby[3], D. Tetzlaff[3,10,11] and J. Karlsson[1]

[1]Climate Impacts Research Centre (CIRC), Department of Ecology and Environmental Science, Umeå University, Linnaeus väg 6, 901 87 Umeå, Sweden.

[2]GET UMR 5563 CNRS, Geoscience and Environment, University of Toulouse, 14 Avenue Edouard Belin, 31400 Toulouse, France.

[3]University of Aberdeen, Kings College, Old Aberdeen, AB24 3UE Aberdeen, Scotland.

[4]Water Resources and Environmental Engineering Research Unit, Faculty of Technology, University of Oulu, PO Box 4300, 900 14 Oulu, Finland.

[5]Organization of the Russian Academy of Sciences A.M. Obukhov Institute of Atmospheric Physics RAS, Pyzhyovskiy pereulok 3, 119 017 Moscow, Russia.

[6]BIO-GEO-CLIM Laboratory, Tomsk State University, Lenina 36, 634 050 Tomsk, Russia.

[7]Institute of Monitoring of Climatic and Ecological Systems (IMCES) SB RAS, Akademichesky Avenue 10/3, 634 055, Tomsk, Russia.

[8]Department of Forest Ecology and Management, The Swedish University of Agricultural Sciences, Skogsmarksgränd 17, 901 83 Umeå, Sweden.

[9]N. Laverov Federal Center for Integrated Arctic Research, IEPS, Russian Academy of Sciences, 23 Nab. Sev. Dviny, Arkhangelsk, Russia.

[10]IGB Leibniz Institute of Freshwater Ecology and Inland Fisheries, Müggelseedamm 310, 125 87 Berlin, Germany.

[11]Humboldt University Berlin, Unter den Linden 6, 100 99 Berlin, Germany.

Abstract

The fate of the vast stocks of organic carbon stored in permafrost of the Western Siberian Lowland, the world's largest peatland, is uncertain. Specifically, the amount of greenhouse gas emissions from rivers in the region is unknown. Here we present estimates of annual CO_2 emissions from 58 rivers across all permafrost zones of the Western Siberian Lowland, between 56 and 67°N. We find that emissions peak at the permafrost boundary and decrease where permafrost is more prevalent and in colder climate conditions. River CO_2 emissions were high, and on average two times greater than downstream carbon export. We suggest that high emissions and emission/export ratios are a result of warm temperatures and long transit times of river water. We show that rivers in the Western Siberian Lowland play an important role in the carbon cycle by degassing terrestrial carbon prior to its transport to the Arctic Ocean, and suggest that changes in both temperature and precipitation are important for understanding and predicting high-latitude river CO_2 emissions in a changing climate.

Large quantities of organic carbon (OC) are stored in permafrost soils in high-latitude regions[1–3]. Recent climate scenarios predict amplified warming of these regions resulting in substantial

43 increase in mean annual air temperatures (MAAT). Such increase will induce widespread
44 permafrost thaw, accelerate release of OC[4] and stimulate its breakdown to carbon dioxide (CO_2)
45 and methane (CH_4) in soils and wetlands[5–7]. Permafrost thawing also increases both the depth of
46 the active layer and the associated release of OC to adjacent running waters[6], where it is partly
47 mineralized and evaded (mainly as CO_2) to the atmosphere. Outgassing of CO_2 from running
48 waters is of significance in the global C cycle[6,8,9]. Yet, the magnitude of river CO_2 emissions is
49 often overlooked, especially in permafrost-affected landscapes where the consequences of
50 climate warming are predicted to be the most severe[3]. Ignoring high-latitude river CO_2 emissions
51 may therefore cause errors in regional and global C budgets and bias assessments of concurrent
52 changes following permafrost thaw.

53 Measurements of C export by major Arctic rivers are relatively common[10,11], whereas the direct
54 measurements of CO_2 emissions from high-latitude rivers are scarce. Available data show that
55 high-latitude rivers are supersaturated in CO_2 and are hotspots for CO_2 release to the
56 atmosphere[12–14]. Bioassays and small scale field studies suggest that OC released from thawing
57 permafrost can be largely degraded in recipient aquatic systems[15,16]. Furthermore, rivers receive
58 and degas CO_2 derived from soil respiration[17], a process accelerated by permafrost thaw[7,18].
59 River CO_2 emissions are therefore important not only for understanding the land-water C
60 exchange with the atmosphere, but also in discerning the degree to which terrestrial C is lost in
61 the aquatic network or exported to downstream coastal areas. This lack of knowledge is
62 particularly evident for Siberia, which has extensive permafrost coverage and associated vast C
63 stocks[1]. In fact, the Western Siberian Lowland (WSL) alone contains 70 Pg C in the region's
64 extensive peatlands[19,20] and is home to the Arctic's largest watershed, the Ob' River, which is the
65 second-largest freshwater contributor to the Arctic Ocean[21]. Moreover, permafrost in the WSL is

highly vulnerable to thaw as its temperature has increased regionally by more than 1°C during the last 30 years[22]. It has been shown recently that WSL permafrost is actively degrading not only within its forest-tundra subzone, but also in its northern tundra subzone[22]. Given the overall sensitivity of permafrost areas to warming, there is a clear need for empirical estimates of CO_2 emissions from permafrost-draining rivers, not least in WSL, to assess their role in regional and global C cycles and the climate system.

Study location and approach

To quantify and compare rates of CO_2 emissions from rivers across different permafrost zones, we examined 58 rivers spanning a latitudinal gradient from 56 to 67°N and covering an area of approximately 1 million km^2 in the WSL (Fig. 1). The rivers had no systematic variation in size or discharge along the latitudinal gradient (Supplementary Fig. 1). We carried out *in-situ* measurements of the partial pressure of CO_2 (pCO_2) and deployed floating chambers[23] to estimate instantaneous CO_2 emissions during spring and summer 2015. All rivers, across all permafrost zones, were supersaturated in pCO_2 with respect to atmosphere, with similar values both in spring (2402 – 5072 µatm) and summer (2187 – 5328 µatm) (Supplementary Tables 1 and 4). The CO_2 emissions varied among the zones (1.9 – 12 g C m^{-2} d^{-1} in spring; 2.7 – 7.6 g C m^{-2} d^{-1} in summer) and showed seasonal differences in the permafrost-free and sporadic permafrost zones (Supplementary Fig. 2, Supplementary Tables 1 and 5). We also estimated diffusive CH_4 emissions from the studied rivers. Although all rivers were net sources of CH_4 to the atmosphere, these emissions were low and constituted only a minor contribution to total atmospheric C emissions, which were dominated by CO_2 (98%).

Annual river CO_2 emissions across permafrost zones

We found strong patterns in annual CO_2 emissions among rivers located in different permafrost zones ($F_{3,54}$ = 6.808, P < 0.05), with three- to five-times greater emissions from rivers where permafrost extent was less than 50% (that is, the permafrost-free and sporadic zones) compared with the continuous permafrost zone (Fig. 2). Annual river CO_2 emissions increased with MAAT throughout permafrost zones (n = 47, r^2 = 0.27, $F_{1,47}$ = 18.05, P < 0.05). Importantly, the highest annual river CO_2 emissions were observed in the sporadic permafrost zone, with a mean value of 1.65 kg C m^{-2} yr^{-1}, which gradually decreased to 0.36 kg C m^{-2} yr^{-1} in the continuous permafrost zone (Fig. 2). Interestingly, this peak occurs at -2 to -4°C MAAT, which coincides with -2°C MAAT isotherm reported by other studies[24–26] marking the border of permafrost appearance. Taken together, the data suggest that warming will result in a general increase in CO_2 emissions from WSL rivers. There are only limited data available on CO_2 emissions from permafrost-draining rivers, but the mean CO_2 emissions for the WSL rivers are 1.5 to 2 times greater than CO_2 emissions reported for rivers in Alaska[12] and Eastern Siberia[13]. A likely explanation for such difference is the higher OC content of WSL soils[2,24–27] compared with Alaska and Eastern Siberia, where soils are more minerogenic[12,13].

Our data suggest that a range of climate-dependent factors interact and control CO_2 emissions across the WSL. Increasing MAAT (Fig. 3) probably elevates CO_2 emissions because of the strong temperature dependency of OC mineralization rates in rivers, but also by extending the ice-free period (Fig. 3) and thus the time window for atmospheric gas exchange. Higher temperatures can also result in elevated CO_2 emissions due to deeper active layers and enhanced export of terrestrial C[11,25,28]. In fact, there is a trend in terrestrial C export (dissolved OC (DOC) + dissolved inorganic carbon (DIC)) with the greatest values observed in the sporadic permafrost zone, where we also see a peak in annual CO_2 emissions from rivers. Yet the differences among

the zones are not significant (Supplementary Table 2), suggesting that impacts of climate on CO_2 emissions are mediated mainly via temperature control of internal OC processing rather than the magnitude of terrestrial C supply. Other factors including nutrients and organic matter quality could not explain the observed differences in CO_2 emissions across permafrost zones (Supplementary Table 3). However, changes in terrestrial C export probably play a role in explaining nonlinear patterns in CO_2 emissions, where the general increase in CO_2 emissions with MAAT throughout permafrost zones reaches a threshold, followed by a decrease in the permafrost-free zone despite higher MAAT and longer ice-free period. Although our study was not designed to examine controls on terrestrial C export across permafrost gradient of the WSL, indicators of water flow pathways based on stable water isotopes (δ^2H and $\delta^{18}O$) (Supplementary Fig. 3) suggest deeper and longer hydrological flow paths[29] in permafrost-free areas, which previously have been shown to lower terrestrial C export as a result of the retention and adsorption of OC in mineral soils[25,30,31]. Thus, lower terrestrial C export may explain the corresponding reduction in CO_2 emissions from permafrost-free rivers, but more in-depth studies are needed to provide a better mechanistic understanding of the control of C cycling and CO_2 emissions from WSL rivers.

River CO_2 emission in relation to downstream C export

To assess the quantitative importance of CO_2 emissions from WSL rivers, we compared annual river CO_2 emissions with river C export across different permafrost zones. We observed overall high emission/export ratios (2 ± 2.2, mean ± interquartile range (IQR)), particularly in the southern permafrost zones, where annual river CO_2 emissions are up to 1.7 – 3 times greater than river C export (Fig. 2, Supplementary Table 2). The low availability of data from other permafrost-affected systems limits our ability to draw firm conclusions, but the ratios for WSL

rivers are relatively high compared to the Yukon River[12] (1:1) and also exceed mean ratios (1.3:1) for the global inland waters[32,33] (Fig. 2). Surprisingly, results for some of the WSL rivers resemble ratios found in the Amazon River (6:1)[12,34]. Although the ratios for WSL rivers contain uncertainties and absolute values should be treated with caution, the results are important and highlight the major role of rivers in the C cycle of the WSL. The differences also emphasize the overall diversity in C dynamics across high-latitude rivers and its potential response to climate change.

High emission/export ratios are unexpected for permafrost-draining rivers, where colder temperatures should constrain mineralization of exported terrestrial OC in recipient waters[12]. Here we suggest that the high emission/export ratios of WSL rivers are a result of long travel times of river water, governed by the overall flat topography of the area[31,35,36], which allows sufficient time for mineralization and outgassing to occur. This effect may be further facilitated by a relatively high degradability of terrestrial OC exported from deeper active layers[15,16], resulting in high total mineralization losses of exported terrestrial OC in the aquatic networks of the WSL. Shorter water travel times, in addition to direct temperature effects on mineralization rates, may also explain the tendency of decreasing emission/export ratios in the northern rivers of the WSL (Fig. 2). In terms of hydrology, the WSL exhibits relatively uniform precipitation (515 ± 80 mm yr^{-1}, mean ± IQR), but lower temperatures in the north decrease evapotranspiration, thus resulting in increasing runoff (Fig. 3) and shorter water travel times. Moreover, the longer ice-cover period in the north implies that the majority of runoff is restricted to a short time window limiting OC mineralization and subsequent CO_2 release. Temperature therefore not only affects C export and processing, but also water travel times by determining the length of the ice-free period and the magnitude of runoff. Again, the permafrost-free zone did not follow the

general trend and showed rather low emission/export ratios, despite higher temperatures and longer water travel times. Here lower emission/export ratios could be a result of decreased export of terrestrial OC versus IC owing to deeper water flow pathways[11]. Although we do not have data on the terrestrial C export ratios, we observed lower DOC/DIC ratios in the permafrost-free zone[31] (Supplementary Table 1), where the higher inorganic fraction of terrestrial C export implies weaker direct temperature and hydrological control of emission/export ratios. This study therefore highlights a complex climate regulation of C cycling in high-latitude rivers where not only changes in temperature *per se*, but also changes in hydrological conditions, are likely to control river CO_2 emissions and emission/export ratios in a changing climate.

Riverine C cycling in permafrost regions

Based on our results we propose a conceptual framework for understanding changes in CO_2 emissions and downstream C export in permafrost-draining rivers with warming (Fig. 4). Warming will raise water temperatures and extend river water travel times, which together will increase CO_2 emissions and emission/export ratios from river networks. The important role of water travel times suggests that changes in temperature, as well as precipitation, will enhance differences in river C fluxes and should be accounted for in assessments of the impacts of climate change. Warming and concurrent active layer deepening are also likely to stimulate terrestrial C export, further increasing river CO_2 emissions. Importantly, as warming progresses and permafrost thaws, deeper flow pathways will possibly decrease terrestrial C export, overriding positive impacts of temperature and water travel times, and therefore resulting in lower CO_2 emissions from rivers. An important implication of this concept is that any warming-induced change in terrestrial C export is largely offset by active processing and degassing in the river network, leaving river C export to the Arctic Ocean relatively unaffected. This emphasizes

the limitation of relying on lateral river C fluxes as an indicator of change in permafrost regions, and instead points to the need for concentrated efforts to assess magnitude and climate control on C emissions from rivers at high latitudes.

References

1. Tarnocai, C. *et al.* Soil organic carbon pools in the northern circumpolar permafrost region. *Global Biogeochem. Cycles* **23,** (2009).

2. Hugelius, G. *et al.* Estimated stocks of circumpolar permafrost carbon with quantified uncertainty ranges and identified data gaps. *Biogeosciences* **11,** 6573–6593 (2014).

3. Schuur, E. A. G. *et al.* Climate change and the permafrost carbon feedback. *Nature* **520,** 171–179 (2015).

4. Crowther, T. W. *et al.* Quantifying global soil carbon losses in response to warming. *Nature* **540,** 104–108 (2016).

5. Smith, L. C. Siberian Peatlands a Net Carbon Sink and Global Methane Source Since the Early Holocene. *Science (80-.).* **303,** 353–356 (2004).

6. Vonk, J. E. *et al.* Reviews and syntheses: Effects of permafrost thaw on Arctic aquatic ecosystems. *Biogeosciences* **12,** 7129–7167 (2015).

7. Dorrepaal, E. *et al.* Carbon respiration from subsurface peat accelerated by climate warming in the subarctic. *Nature* **460,** 616–619 (2009).

8. Vonk, J. E. & Gustafsson, Ö. Permafrost-carbon complexities. *Nat. Geosci.* **6,** 675–676 (2013).

9. Cole, J. J. *et al.* Plumbing the Global Carbon Cycle: Integrating Inland Waters into the Terrestrial Carbon Budget. *Ecosystems* **10,** 172–185 (2007).

10. Cooper, L. W. *et al.* Flow-weighted values of runoff tracers (δ18O, DOC, Ba, alkalinity) from the six largest Arctic rivers. *Geophys. Res. Lett.* **35,** 3–7 (2008).

11. Striegl, R. G., Aiken, G. R., Dornblaser, M. M., Raymond, P. A. & Wickland, K. P. A decrease in discharge-normalized DOC export by the Yukon River during summer through autumn. *Geophys. Res. Lett.* **32,** L21413 (2005).

12. Striegl, R. G., Dornblaser, M. M., McDonald, C. P., Rover, J. R. & Stets, E. G. Carbon dioxide and methane emissions from the Yukon River system. *Global Biogeochem. Cycles* **26,** (2012).

13. Denfeld, B. A., Frey, K. E., Sobczak, W. V., Mann, P. J. & Holmes, R. M. Summer CO_2 evasion from streams and rivers in the Kolyma River basin, north-east Siberia. *Polar Res.* **32,** 1–15 (2013).

14. Lundin, E. J., Giesler, R., Persson, A., Thompson, M. S. & Karlsson, J. Integrating carbon emissions from lakes and streams in a subarctic catchment. *J. Geophys. Res. Biogeosciences* **118,** 1200–1207 (2013).

15. Abbott, B. W., Larouche, J. R., Jones, J. B., Bowden, W. B. & Balser, A. W. Elevated dissolved organic carbon biodegradability from thawing and collapsing permafrost. *J. Geophys. Res. G Biogeosciences* **119,** 2049–2063 (2014).

16. Vonk, J. E. *et al.* High biolability of ancient permafrost carbon upon thaw. *Geophys. Res. Lett.* **40,** 2689–2693 (2013).

17. Dubois, K. D., Lee, D. & Veizer, J. Isotopic constraints on alkalinity, dissolved organic carbon, and atmospheric carbon dioxide fluxes in the Mississippi River. *J. Geophys. Res. Biogeosciences* **115,** (2010).

18. Knoblauch, C., Beer, C., Sosnin, A., Wagner, D. & Pfeiffer, E. M. Predicting long-term carbon mineralization and trace gas production from thawing permafrost of Northeast

Siberia. *Glob. Chang. Biol.* **19,** 1160–1172 (2013).

19. Sheng, Y. *et al.* A high-resolution GIS-based inventory of the west Siberian peat carbon pool. *Global Biogeochem. Cycles* **18,** (2004).

20. Frey, K. E., Siegel, D. I. & Smith, L. C. Geochemistry of west Siberian streams and their potential response to permafrost degradation. *Water Resour. Res.* **43,** (2007).

21. Frappart, F. *et al.* Interannual variations of the terrestrial water storage in the Lower Ob' Basin from a multisatellite approach. *Hydrol. Earth Syst. Sci.* **14,** 2443–2453 (2010).

22. Romanovsky, V. E. *et al.* Thermal state of permafrost in Russia. *Permafr. Periglac. Process.* **21,** 136–155 (2010).

23. Alin, S. R. *et al.* Physical controls on carbon dioxide transfer velocity and flux in low-gradient river systems and implications for regional carbon budgets. *J. Geophys. Res.* **116,** G01009 (2011).

24. Frey, K. E. Amplified carbon release from vast West Siberian peatlands by 2100. *Geophys. Res. Lett.* **32,** L09401 (2005).

25. Frey, K. E. & McClelland, J. W. Impacts of permafrost degradation on arctic river biogeochemistry. *Hydrol. Process.* **23,** 169–182 (2009).

26. Frey, K. E., McClelland, J. W., Holmes, R. M. & Smith, L. C. Impacts of climate warming and permafrost thaw on the riverine transport of nitrogen and phosphorus to the Kara Sea. *J. Geophys. Res. Biogeosciences* **112,** (2007).

27. Hugelius, G. *et al.* The Northern Circumpolar Soil Carbon Database: spatially distributed datasets of soil coverage and soil carbon storage in the northern permafrost regions. *Earth Syst. Sci. Data* **5,** 3–13 (2013).

28. Algesten, G. *et al.* Role of lakes for organic carbon cycling in the boreal zone. *Glob. Chang. Biol.* **10,** 141–147 (2004).

29. Ala-aho, P. *et al.* Using stable isotopes to assess surface water source dynamics and hydrological connectivity in a high-latitude wetland and permafrost influenced landscape. *J. Hydrol.* **556,** 279–293 (2017).

30. Kawahigashi, M., Kaiser, K., Kalbitz, K., Rodionov, A. & Guggenberger, G. Dissolved organic matter in small streams along a gradient from discontinuous to continuous permafrost. *Glob. Chang. Biol.* **10,** 1576–1586 (2004).

31. Pokrovsky, O. S. *et al.* Permafrost coverage, watershed area and season control of dissolved carbon and major elements in western Siberian rivers. *Biogeosciences* **12,** 6301–6320 (2015).

32. Raymond, P. A. *et al.* Global carbon dioxide emissions from inland waters. *Nature* **503,** 355–359 (2013).

33. Lauerwald, R., Laruelle, G. G., Hartmann, J., Ciais, P. & Regnier, P. A. G. Spatial patterns in CO 2 evasion from the global river network. *Global Biogeochem. Cycles* **29,** 534–554 (2015).

34. Richey, J. E., Melack, J. M., Aufdenkampe, A. K., Ballester, V. M. & Hess, L. L. Outgassing from Amazonian rivers and wetlands as a large tropical source of atmospheric CO2. *Nature* **416,** 617–620 (2002).

35. Zakharova, E., Kouraev, A. V., Rémy, F., Zemtsov, V. & Kirpotin, S. N. Seasonal variability of the Western Siberia wetlands from satellite radar altimetry. *J. Hydrol.* **512,** 366–378 (2014).

36. Smith, L. C. *et al.* Influence of permafrost on water storage in West Siberian peatlands revealed from a new database of soil properties. *Permafr. Periglac. Process.* **23,** 69–79 (2012).

37. Brown, J., O.J.J. Ferrians, J.A. Heginbottom & E.S. Melnikov. Circum-Arctic Map of Permafrost and Ground Ice Conditions. (2001).

Acknowledgments

The study was part of the JPI Climate initiative, financially supported by VR (the Swedish Research Council) grant no. 325-2014-6898 to J.K. Additional funding from the RNF (RSCF) grant no. 18-17-00237, RFBR grant no. 17-55-16008 and RF Federal Target Program RFMEFI58717X0036 “Kolmogorov” to O.S.P. and S.N.K. as well as NERC grant no. NE/M019896/1 to C.S. are acknowledged. The authors thank A. Sorochinskiy and A. Lim for assistance in the field as well as M. Myrstener, M. Klaus and S. Monteux for advice on data analysis. L. Kovaleva is acknowledged for artwork.

Author contribution

J.K. and O.S.P. contributed to study design. S.N.K. organized sampling campaigns and logistics. S.S., R.M.M., I.V.K. and V.K. contributed to sampling. L.S.S. analyzed DOC and DIC samples. S.G.K. complemented data with literature material. S.S. analyzed data, prepared figures and tables. S.S., J.K., O.S.P. and H.L. wrote the paper. C.S., D.T. and P.A. helped with interpreting results. All authors commented on the manuscript.

Competing interests

The authors declare no competing interests.

Corresponding author

Correspondence and requests for materials should be addressed to S.S. or J.K.

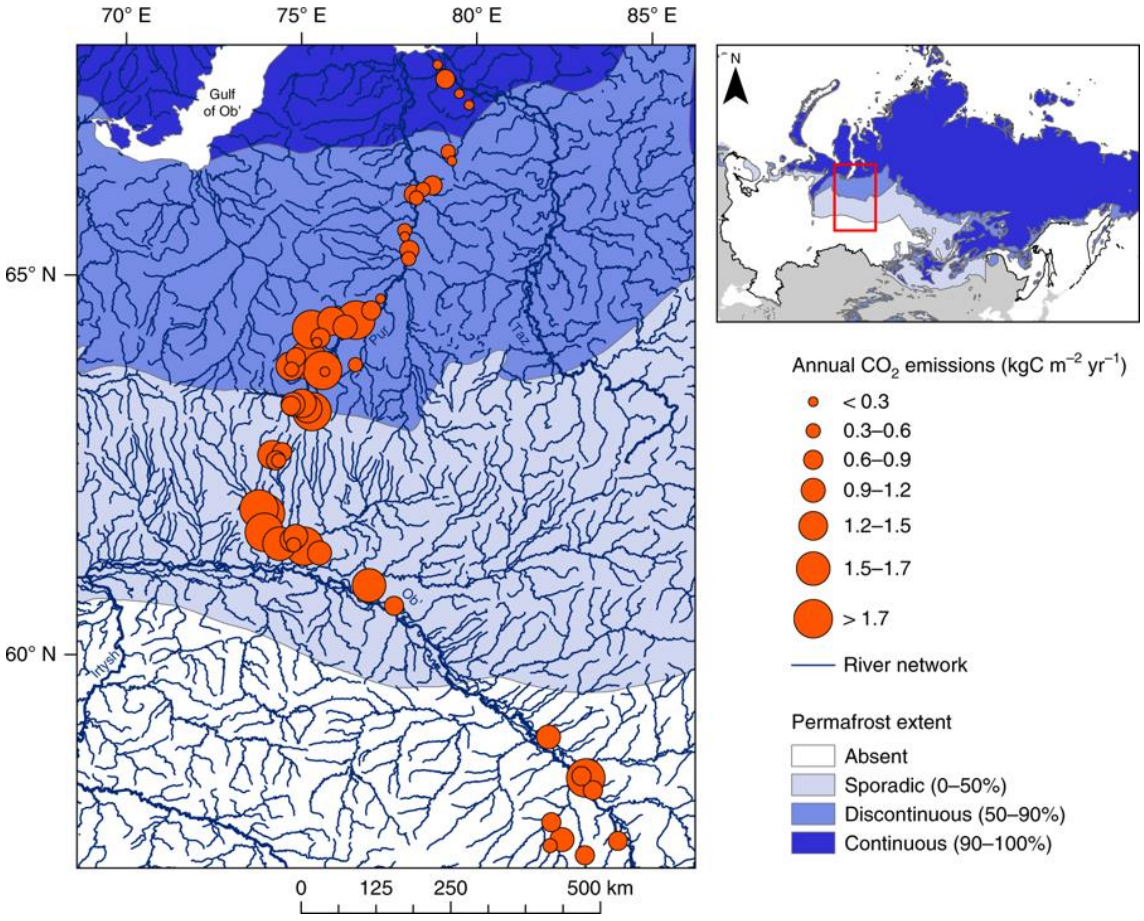

299

300 **Fig. 1. Map of the study sites in the WSL, Russia.** The blue shading represents permafrost
301 extent in the WSL based on published data[6,37], while the size of the orange circles represents the
302 magnitude of the annual CO_2 emissions (per unit water area) from the studied rivers.

303

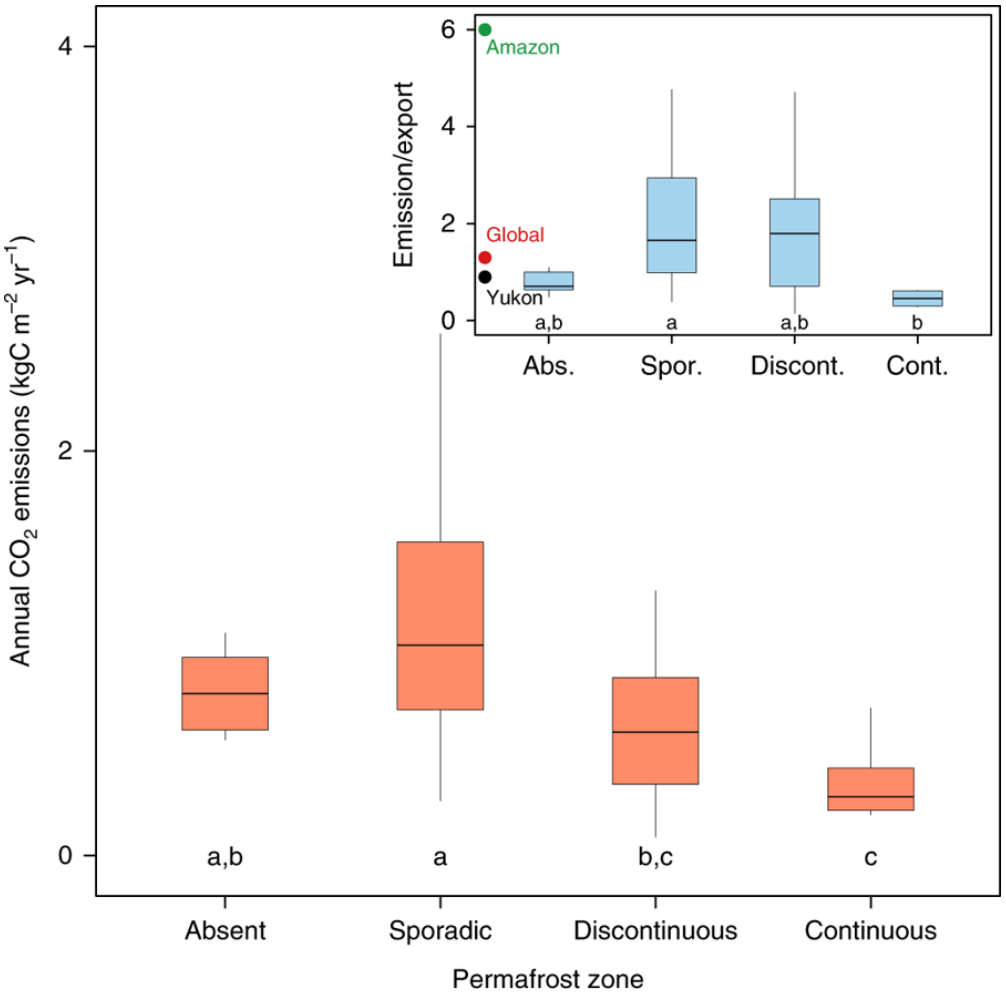

304

305 **Fig. 2. Annual river CO_2 emissions per unit water area across different permafrost zones.**
306 Annual river CO_2 emissions increase with permafrost extent and reach maximum values in the
307 sporadic permafrost zone subsequently declining as permafrost becomes more prevalent. The
308 inset shows C emission/export ratios across permafrost zones and mean emission/export ratios
309 for Amazon[36], Yukon[12] and global river network[32,33] (assuming 0.9 Pg annual river C export to
310 the oceans). Boxes are bound by 25th and 75th percentiles and whiskers show 1.5 IQR. Middle
311 line represents median values. Permafrost zones that share a letter are not significantly different.
312 For sample sizes, see Supplementary Table 2.

313

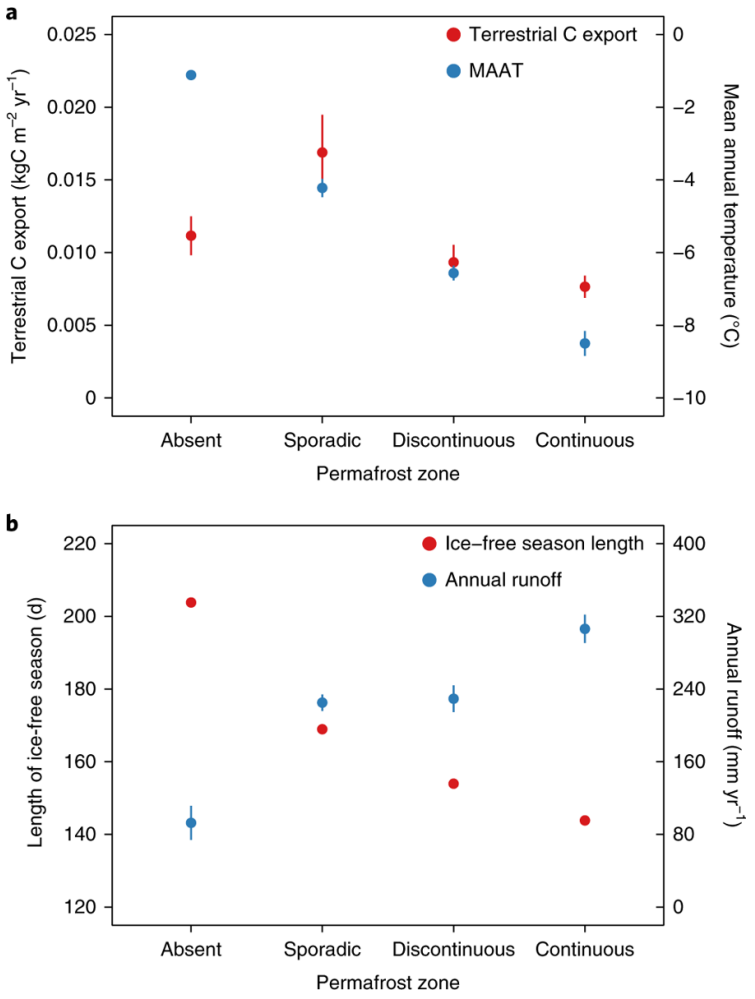

314

315 **Fig. 3. Climate-dependent factors controlling river CO_2 emissions across different**
316 **permafrost zones. (a)** Terrestrial C export (left y axis) and mean annual temperature (right y
317 axis), **(b)** The length of ice-free season (left y axis) and mean annual runoff (right y axis) across
318 permafrost zones. Dots represent mean values, whereas whiskers indicate the standard error of
319 the mean (s.e.m). For sample sizes, see Supplementary Table 2.

320

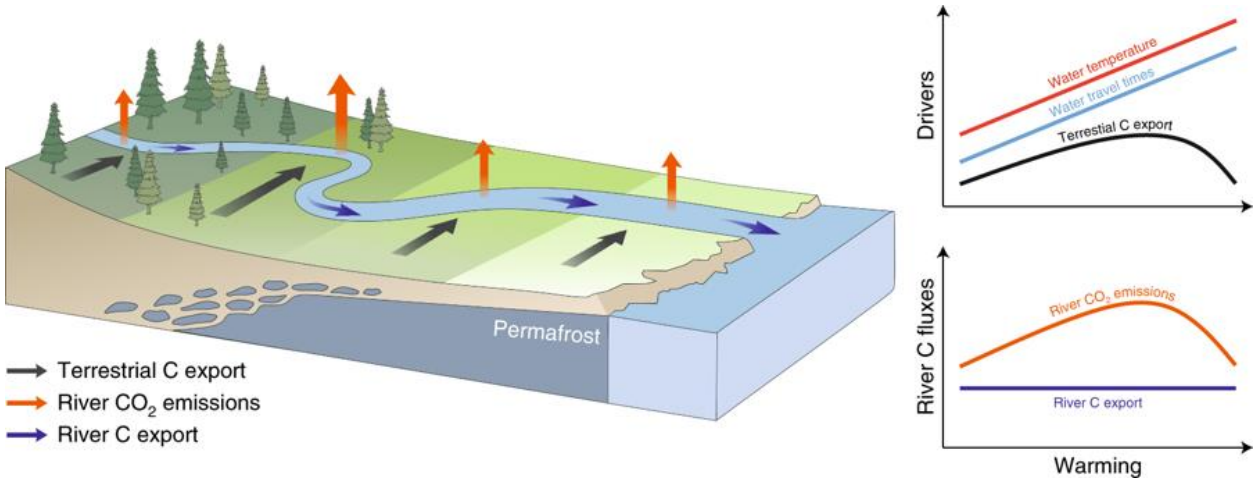

321

322 **Fig. 4. A conceptual model for changes in CO_2 emissions and downstream C export from**
323 **permafrost-draining river network with warming.** Warming raises water temperatures and
324 extends river water travel times, resulting in increases in CO_2 emissions and emission/export
325 ratios from river networks. Warming and associated permafrost thaw will probably also stimulate
326 terrestrial C export, thus further enhancing riverine C fluxes. As warming progresses and
327 permafrost disappears, terrestrial C export decreases, counteracting effects by temperature and
328 water travel times, and leading to decrease in river CO_2 emissions.

329

Methods

Sampling sites. The three studied river basins, Ob', Pur and Taz, are located in the WSL (Russia) between the southern taiga (56 °N) and the tundra (67 °N) ecotones and represent an area of over 2,000,000 km^2. Because of its geographical location and size, the region is distinct in terms of the latitudinal and zonal variation of climate and permafrost extent. The climate is moderate continental with the MAAT ranging from approximately –0.5°C in the south to –9.5°C in the north, and mean annual precipitation ranging from 477 ± 10 mm yr^{-1} (mean ± IQR) to 444 ± 11 mm yr^{-1} (mean ± IQR), accordingly[31]. Permafrost is widespread and occupies the greater part of the WSL, stretching from the polar circle to the shores of the Arctic Ocean over 1,000 km distance[20,25]. The duration of the ice cover period varies latitudinally from five months in the south to more than seven months in the north[38]. The WSL is characterized by a low and flat relief (0 – 200 masl)[39] and is dominated by Pliocene sands and clays overlain by a layer of peat (~1 – 3 m)[31]. The thickness of seasonally frozen soil varies from 1.7 – 2 m in the south (56 °N) to less than 0.8 m in the north (66 °N)[40]. We sampled 58 streams and rivers spanning a wide range of watershed sizes and permafrost extent. The catchment areas of the sampled rivers ranged from 2 to 150,000 km^2, but exhibited relatively uniform morphometry. The water flow was calm and lacked turbulence throughout the river course even at peak discharge, due to the overall flat terrain of the WSL[31]. Our sampled sites showed no systematic variation in watershed size, discharge or landscape characteristics such as the proportion of bogs or forests across different permafrost zones (for details on statistics see Statistical analysis section below). We visited all sites during spring (10 – 25 June) and summer (21 July – 19 August) 2015. The timing of the two sampling campaigns covered approximately 80% of annual water discharge in the basins[38], and therefore was assumed to be representative for the open water season.

Water chemistry. At each location, pH, water temperature, dissolved oxygen saturation and specific conductivity were measured below the water surface using a WTW multiparameter (uncertainty ± 5%). The probes were calibrated every other day using a two-point calibration technique with standard buffer solutions. Air temperature and atmospheric pressure were measured using ADC Summit handheld weather station (Silva). Water samples for DOC, DIC, nutrients, total nitrogen (TN) and total phosphorus (TP) (50 ml) were collected 1 – 2 m offshore using vinyl gloves and pre-washed polypropylene jars. Samples for DOC and DIC were filtered immediately on site using sterile plastic syringes in clean 30 ml polypropylene Nalgene bottles through single-use pre-washed acetate cellulose filter units (Minisart, Sartorius; 0.45 μm pore size, 33 mm diameter). The first 20 – 50 ml of filtrate were discarded. DOC and DIC samples were refrigerated in the dark until analysis by high-temperature catalytic oxidation using a total organic carbon (TOC) analyzer, Shimadzu (uncertainty ± 3%; 0.1 mg l^{-1} detection limit). The DOC blanks of filtrate never exceeded 0.1 mg l^{-1}. Water samples for NH_4^+-N, NO_3^--N, and PO_4^{-3}-P were filtered on site through pre-combusted (at 550° C for 4h) acid-washed glass fiber filters (0.45 μm, Whatman Arbor Technologies, USA) and were also stored frozen in the dark until analyses. These were analyzed at Umeå University using an automated flow injection analyzer (FIA star 5000, FOSS) with the detection limits 1 μg l^{-1} for NH_4^+-N, 0.5 μg $^{-1}$ for NO_3^--N and 0.5 μg $^{-1}$ for PO_4^{-3}-P, whereas total nitrogen and total phosphorus were analysed using IL 550 TOC/total N analyzer with the detection limit of 50 μg l^{-1} (Hach-Lange GmbH). Water samples for dissolved CH_4 were collected in a 20 ml gas-tight vial closed without air bubbles using vinyl stoppers and aluminium caps. 0.2 ml of saturated $HgCl_2$ was injected into the vial using two-way needle system. Samples were stored in the dark until analysis in the laboratory at Tomsk State University, where a headspace was made by displacing approximately 40% of water with N_2

(99.999%) and creating two 0.5 ml replicate samples. These were analyzed using Bruker GC-456 gas chromatograph equipped with a flame ionization and thermal conductivity detectors. Calibration of the detectors was performed after every tenth sample using air liquid gas standards of known concentrations (0, 145 ppmv CH_4). The reproducibility of results was within ± 5%. Molar concentrations of CH_4 were calculated by using temperature-specific solubility coefficients as in Yamamoto and colleagues[41]. Because summer concentrations of dissolved CH_4 were generally low (0.02 ± 0.02, mean ± IQR) and constituted roughly 2% of total summer C emissions, the data on CH_4 emissions are not discussed here. We further measured ultraviolet absorbance at 245 nm (UV_{245}) using a 1 cm quartz cuvette in a CARY-50 UV-Vis spectrophotometer (Bruker). These values were later converted to UV_{254}[42]. We calculated specific ultraviolet absorbance ($SUVA_{254}$) of the sampled water which served as a proxy for aromatic C and organic matter quality in river water.

***p*CO₂** Surface water pCO_2 was measured *in situ* by deploying a hand-held infrared gas analyzer (IRGA, GMT222 CARBOCAP probe, Vaisala; accuracy ± 1.5%) with various detection ranges (2 000, 10 000, 20 000 ppm) enclosed within a waterproof and gas-permeable membrane. During the sampling, the hand-held meter was placed directly into the water column of a sampled stream, where it was allowed to equilibrate for approximately 10 min. If the measurements were 1.5% outside the sensor's range, it was replaced with another sensor that had higher range. Sensor preparation was conducted in the lab following the method described by Johnson and colleagues[43]. The hand-held measurement indicator unit (MI70, Vaisala; accuracy ± 0.2%) was connected to the sensor allowing instantaneous readings of pCO_2. Replicated measurements were taken at each site to minimize uncertainty. The sensors were calibrated linearly in the lab against standard gas mixtures (0, 800, 3 000, 8 000 ppm; $r^2 > 0.99$) after the sampling. The sensors' drift

was 0.03 – 0.06% per day and the overall error was 4 – 8% (relative s.d.). Following calibration, the post-measurement correction of the sensor output induced by changes in water temperature and barometric pressure was done by applying empirically derived coefficients following Johnson and colleagues[43]. Finally, temperature-specific solubility coefficients were used to calculate respective CO_2 concentrations in the water as in Wanninkhof and colleagues[44].

CO_2 flux calculations. The flux of CO_2 (f_{CO_2}) was calculated using the following equation (equation (1)):

$$f_{CO_2} = K_h \, k_{CO_2} \, (C_{water} - C_{air}), \qquad (1)$$

where K_h is Henry's constant corrected for temperature and pressure (in mol l^{-1} atm^{-1}), k_{CO_2} is the gas exchange velocity at a given temperature (in cm h^{-1}), C_{water} is the water CO_2 concentration, and C_{air} is the CO_2 concentration in the ambient air.

To measure k_{CO_2}, we used a floating chamber. The chamber was made of a plastic bin (30 cm length × 25 cm width × 15 cm height; volume 7.02 l) fitted with floats and covered with aluminium tape to minimize surface heating. The chamber was connected to an IRGA and a pump (GM70, Vaisala) in a closed loop via CO_2-impermeable tubing with an intervening moisture trap. The pump was used to circulate air to the IRGA during the measurement period. The hand-held measurement indicator unit (MI70, Vaisala; accuracy ± 0.2%) was attached to the system and used for recording values during the sampling. Before the chamber was deployed, it was flushed with ambient air for roughly 20 – 30 sec. The chamber was gently placed on the water surface near the shore to avoid inducing artificial turbulence. The CO_2 accumulation rate inside the chamber was recorded continuously at 1 – 10 s interval for 5 – 10 minutes. Measurements were repeated two to three times in different parts of the channel for each location, when possible. If the river shore allowed free access, chamber measurements were

performed by allowing it to drift freely with the river current for some 50 – 200 m while recording. In four of the rivers, where mean annual discharge is higher than 100 m^3 s^{-1} (Ob', Pyakupur, Pur and Taz), the measurements were made by deploying the chamber alongside a boat during free drift. Measurements were repeated two to three times at each of the locations where the chamber could drift. The rate of CO_2 accumulation was computed by linear regression. Although 94% of the measurements had a linear increase with $r^2 > 0.80$, 8% of the measurement had a linear increase with $r^2 < 0.80$. These measurements were retained if the replicates existed and if the average r^2 between the replicates was greater than 50%. We further corrected for overestimation of the CO_2 accumulation rate inside the static chamber for each of the rates separately by multiplying with the factor derived from average percent difference between drifting and static chamber measurements. We manually trimmed readings from drifting chambers leaving only those, where percent difference was negative (that is, static chamber measurements were greater than the ones obtained from a drifting chamber). We performed corrections for each of the sampled sites and sampling seasons separately. The correction reduced our measured CO_2 emissions on average by 33% in spring and by 62% in summer, but did not affect the differences in annual CO_2 emissions among permafrost zones. On four rivers (Ob', Pyakupur, Pur and Taz), we also measured pCO_2 and CO_2 emissions along with other water chemistry parameters (pH, conductivity, dissolved O_2 and so on) from transects (4 – 5 points) across the river channel. None of the measured parameters varied across the river channel for the corresponding rivers.

We estimated instantaneous CO_2 fluxes by modifying equation (1) and using slopes of the CO_2 accumulation in the chambers (equation (2)):

$$f_{CO_2} = K_h \, h \left(\frac{d(pCO_2)}{dt}\right), \qquad (2)$$

where h is chamber's mean height (in m) while $d(pCO_2)/dt$ is the slope of CO_2 accumulation in the chamber over time (in ppm s^{-1})[23,45]. The k_{CO_2} values were then calculated by inverting equation (1) and isolating k_{CO_2} (equation (3))[45]:

$$k_{CO_2} = \frac{f_{CO_2}}{K_h\,(pCO_{2_{water}} - pCO_{2_{air}})}, \qquad (3)$$

where $pCO_{2_{water}}$ is the CO_2 concentration in the water (in ppm), and $pCO_{2_{air}}$ is the CO_2 air-water equilibrium concentration, which is set to 400 ppm, the average global atmospheric CO_2 concentration during 2015. To compare gas transfer velocities among sites, calculated k_{CO_2} values were then standardized to a Schmidt number of 600 using equation (4)[23,45]:

$$k_{600} = k_{CO_2}\left(\frac{600}{Sc_{CO_2}}\right)^{-n}, \qquad (4)$$

where Sc_{CO_2} is the CO_2 Schmidt number for a given temperature[45], exponent n is a coefficient that describes the water surface (2/3 for a smooth water surface regime, 1/2 for a rippled and a turbulent one), and the Schmidt number for 20°C in freshwater is 600[23,46]. We used *n*=2/3 because all water surfaces of the sampled rivers were considered flat and had a laminar flow. Finally, we calculated k_{CH_4} and used these values to estimate instantaneous CH_4 emissions for the respective rives.

Stable water isotopes. Samples for stable water isotopes (δ^2H and $\delta^{18}O$) were taken in the middle of the river channel, or from the river bank at the depth of 0.5 m within the actively flowing water. All samples were collected into 3.5 ml glass vials and stored in the dark at 4 – 6°C until analysis. These were analysed at the University of Aberdeen using a Los Gatos DLT-100 laser isotope analyzer with an instrument precision of ± 0.4‰ for δ^2H and ± 0.1‰ for $\delta^{18}O$. Isotope ratios are reported in the δ-notation using the Vienna Standard Mean Ocean Water standards.

Ancillary data. We used data on mean annual discharge, annual runoff, catchment area and proportion of bogs, lakes, forest coverage and permafrost extent for each location from Pokrovsky and colleagues[31]. We complemented this data with data on the MAAT, mean annual precipitation, mean length of ice cover season and topography of the watersheds using data available in the Russian literature[47,48].

Annual river CO_2 emission. We quantified annual river CO_2 emission as the product of mean seasonal CO_2 emission and number of ice-free days for the respective rivers. As the number of sampled rivers in the area where permafrost is absent (referred to as the 'absent' permafrost zone) varied between the seasons (n=6 for spring and n=8 for summer) and some of the rivers were sampled during only one of the seasons, we assumed seasonal differences to be negligible for such rivers and used existing values when quantifying annual river CO_2 emission (yielding a total n=9 for absent area). We, however, excluded such rivers when analyzing seasonal differences in river CO_2 emission within each of the permafrost zones (see Statistical analysis section).

Water surface area. We modelled the water surface area of the respective rivers by using published relationships between the natural log of percent stream surface area and the natural log of mean annual precipitation and MAAT for the watersheds above 60 °N[32] (see Raymond and colleagues[32];):

$$\ln(\%SA) = \ln P \ 1.04 - 5.01e^{-2}\, T - 7.08\,, \qquad (5)$$

where $\ln(\%SA)$ is the natural log of the percentage of stream surface area, $\ln P$ is the natural log of mean annual precipitation in the watershed (in mm yr^{-1}) while T is the MAAT (in °C). These calculated water surface areas were used to derive annual areal CO_2 emissions for each of the studied sites. We acknowledge our estimate is rather conservative, but highlight it as being

realistic in reflecting summer base flow conditions for WSL rivers. It is likely that we underestimate the areas because of large proportion of inundated floodplains during the spring flood, when the flooded area ratio on average is 85% for WSL rivers excluding Taz[38]. These are not accounted for in water surface areas calculations that largely rely on data of interannual average of air temperature and precipitation in the respective catchments. However, we do not attempt to derive high-resolution numbers; we rather seek to explore more general basin-scale patterns that are not affected by year-to-year variability.

River C export and terrestrial C export. We quantified river C export for each of the studied sites as the product of summer DOC and DIC concentrations and site-specific discharge. Comparing our values for organic C export (kg m^{-2} yr^{-1}) with previously published estimates for three of our WSL sites (Ob, Pur and Taz) measured at the rivers' outlets[10,31,49] gave similar results (1.7 ± 0.3, mean of the difference ± IQR of the difference). Using a mass balance approach, we calculated terrestrial C export for each catchment as the product of annual river CO_2 emissions and river C export.

Statistical analysis. Before statistical analyses, we grouped the sampled rivers on the basis of the sampling location in four categories that represent different permafrost zones: (1) absent (≤ 59 °N, n=9), (2) sporadic (60 – 63 °N, n=27), (3) discontinuous (64 – 65 °N, n=16) and (4) continuous (> 65 °N, n=6). We merged isolated and sporadic permafrost zones together under sporadic permafrost group as done elsewhere[6]. We also grouped the sampled sites into four different classes that represent watershed sizes: (1) small (< 100 km^2, n=19), (2) intermediate (100 – 1 000 km^2, n=20), (3) big (1 000 – 10 000 km^2, n=10) and (4) huge (> 10 000 km^2, n=9). All statistical analyses were performed in RStudio statistical software (Version 1.0.44, RStudio, Inc.; www. r-project.org).

To meet the normality assumption, all variables were log-transformed when necessary. The normality of data distribution was assessed by Shapiro-Wilk normality test. We further checked for the homogeneity of variances between the groups by using parametric Bartlett test. We used one-way analysis of variance (ANOVA) with Tukey's HSD post-hoc comparisons to investigate differences in annual river CO_2 emissions among permafrost zones. All variables and their residuals followed normal distributions after transformation.

We further used linear mixed effects models (lme4 package) when analyzing two-way interactions of seasons and permafrost zones on the transformed per unit area daily CO_2 emissions and surface water pCO_2. We used permafrost zones and seasons as fixed factors that are expected to have a systematic influence on the data, while we allowed our sampled streams to randomly vary inside permafrost zone groups and watershed classes, as well as months inside permafrost zone groups, to correct for the nested design of the study and resolve interdependency issue. In that way, we assumed that whatever the effects of permafrost extent and seasons are, they are going to be the same for all rivers sampled within the permafrost zone group. The best model fit was selected based on Akaike information criterion (AIC). We also performed contrasts analyses on respective mixed effects models by constructing orthogonal contrasts to compare seasons between each other and avoid multiple comparisons (lsmeans package).

We used linear regression when analyzing the relationship between annual CO_2 emissions and MAAT. We also run multiple regression analysis on the dataset to see which of the variables (discharge, annual runoff, proportion of bogs, lakes, forest coverage and permafrost extent and so on) might be good predictors of the seasonal and annual CO_2 emissions. No linear combination of the variables gave r^2 greater than 50%.

We further tested the variation in watershed size, discharge or landscape characteristics such as the proportion of bogs and forest coverage among different permafrost zones groups by using ANOVA with Tukey's HSD post-hoc comparison or a non-parametric alternative of the Pairwise Wilcox test with the Holm adjustment. None of the variables exhibited significant differences between permafrost zones. We also used parametric Levene's test on homogeneity of variances when assessing the variability in δ^2H and $\delta^{18}O$ between permafrost zones as well as pairwise Wilcox test with the Holm adjustment when examining differences in terrestrial C export between permafrost zones.

Note that we report untransformed data in the text, figures and tables. Because of the non-normal distribution of the data, we use mean ± IQR when reporting uncertainty. All statistical tests used a significance level of 5% ($\alpha = 0.05$) and were run on the complete dataset including all rivers. We remove outliers in Fig. 2 to visually improve the graph.

Data Availability. A summary of data generated and analyzed during this study is available in the Supplementary Information Files. Water chemistry parameters and watershed characteristics for each of the sampled rivers are available as a separate Excel file. Additional pCO_2 and CO_2 emission data for each of the studied rivers are available upon request.

References

38. Zakharova, E. A. A. *et al.* The modern hydrological regime of the northern part of Western Siberia from in situ and satellite observations. *Int. J. Environ. Stud.* **66,** 447–463 (2009).

39. Karlsson, J. M., Lyon, S. W. & Destouni, G. Thermokarst lake, hydrological flow and water balance indicators of permafrost change in Western Siberia. *J. Hydrol.* **464–465,**

459–466 (2012).

40. Raudina, T. V. *et al.* Dissolved organic carbon and major and trace elements in peat porewater of sporadic, discontinuous, and continuous permafrost zones of western Siberia. *Biogeosciences* **14,** 3561–3584 (2017).

41. Yamamoto, S., Alcauskas, J. B. & Crozier, T. E. Solubility of methane in distilled water and seawater. *J. Chem. Eng. Data* **21,** 78–80 (1976).

42. Cuthbert, I. D. & del Giorgio, P. Toward a standard method of measuring color in freshwater. *Limnol. Oceanogr*. **37,** 1319–1326 (1992).

43. Johnson, M. S. *et al.* Direct and continuous measurement of dissolved carbon dioxide in freshwater aquatic systems-method and applications. *Ecohydrology* **3,** (2009).

44. Wanninkhof, R. Relationship between wind speed and gas exchange over the ocean. *J. Geophys. Res.* **97,** 7373–7382 (1992).

45. Vachon, D., Prairie, Y. T. & Cole, J. J. The relationship between near-surface turbulence and gas transfer velocity in freshwater systems and its implications for floating chamber measurements of gas exchange. *Limnol. Oceanogr.* **55,** 1723–1732 (2010).

46. Jähne, B., Heinz, G. & Dietrich, W. Measurement of the diffusion coefficients of sparingly soluble gases in water. *J. Geophys. Res. Ocean.* **92,** 10767–10776 (1987).

47. Nikitin, S. P. & Zemtsov, V. A. The Variability of Hydrological Parameters of Western Siberia. Nauka, Novosibirsk, 204 pp., (1986) (available in Russian literature).

48. Novikov, S. M. et al. Hydrology of Bog Territories of the Permafrost Zone of Western Siberia. BBM publishing House, St. Petersburg, 535 pp., (2009) (available in Russian literature).

49. Gordeev, V. V., Martin, J. M., Sidorov, I. S. & Sidorova, M. V. A reassessment of the Eurasian river input of water, sediment, major elements, and nutrients to the Arctic Ocean. *Am. J. Sci.* **296,** 664–691 (1996).